

Identifying noise transients in gravitational-wave data arising from nonlinear couplings

Bernard Hall¹, Sudhagar Suyamprakasam^{2,3}, Nairwita Mazumder¹, Anupreeta More², Sukanta Bose^{1,2}

¹ Department of Physics & Astronomy, Washington State University 1245 Webster, Pullman, WA 99164-2814, U.S.A

² Inter-University Centre for Astronomy and Astrophysics, Post Bag 4, Ganeshkhind, Pune 411 007, India

³ Nicolaus Copernicus Astronomical Center, Polish Academy of Sciences, Bartycka 18, 00-716, Warsaw, Poland

E-mail: sukanta@wsu.edu

LIGO Document Number: P2200344

Abstract. Noise in various interferometer systems can sometimes couple non-linearly to create excess noise in the gravitational wave (GW) strain data. Third-order statistics, such as bicoherence and biphas, can identify these couplings and help discriminate those occurrences from astrophysical GW signals. However, the conventional analysis can yield large bicoherence values even when no phase-coupling is present, thereby, resulting in false identifications. Introducing artificial phase randomization in computing the bicoherence reduces such occurrences with negligible impact on its effectiveness for detecting true phase-coupled disturbances. We demonstrate this property with simulated disturbances – focusing only on short-duration ones (lasting up to a few seconds) in this work. Statistical hypothesis testing is used for distinguishing phase-coupled disturbances from non-phase coupled ones when employing the phase-randomized bicoherence. We also obtain an expression for the bicoherence value that minimizes the sum of the probabilities of false positives and false negatives. This can be chosen as a threshold for shortlisting bicoherence triggers for further scrutiny for the presence of non-linear coupling. Finally, the utility of the phase-randomized bicoherence analysis in GW time-series data is demonstrated for the following three scenarios: (1) Finding third-order statistical similarities within categories of noise transients, such as blips and koi fish. If these non-Gaussian noise transients, or glitches, have a common source, their bicoherence maps can have similarities arising from common bifrequencies related to that source. (2) Differentiating linear or non-linear phase-coupled glitches from compact binary coalescence signals through their bicoherence maps. This is explained with a simulated signal. (3) Identifying repeated bifrequencies in the second and third observation runs (i.e., O2 and O3) of LIGO and Virgo.

Keywords: Noise-artifacts, Non-linear Couplings, Bispectrum, Bicoherence, Binary Black Holes

1. Introduction

The detectors of the Laser Interferometer Gravitational-wave Observatory (LIGO) [1], Virgo [2] and the Kamioka Gravitational Wave Detector (KAGRA) [3] are among the most sophisticated scientific instruments in the world. To date, LIGO and Virgo have detected several dozens of gravitational wave (GW) signals [4, 5, 6, 7] from colliding binaries involving black holes and neutron stars. These detectors on the globe are sensitive to GW signals in the $10 - 10^4$ Hz band [8], but are often plagued by unwanted noise transients from various terrestrial sources, which can adversely impact that sensitivity [9, 10, 11, 12]. The quality of data or search sensitivity can be improved by removing or minimizing the noise transients in the instruments, whenever possible. It is, however, non-trivial to do so because the origins of many of them are unknown or, in some cases, not in our control (e.g., earthquakes) [13]. Those difficulties notwithstanding, detector characterization exercises and related data-analysis techniques have been employed for mitigating several kinds of noise transients in GW searches [14, 15, 16]. In some of these cases the excess noise-power in the GW strain-data is due to bilinear or nonlinear couplings among various detector subsystems and components [17, 18, 19, 20, 21, 22]. Whenever the causes of disturbances are found, steps are taken to remove or reduce their impact on the GW strain channel and the detector's sensitivity to astrophysical signals.

In this work, we develop a technique for detecting the presence of nonlinear couplings at second order, i.e., quadratic nonlinearities, in the GW strain data. A third-order statistic that is useful for such identification is the *bicoherence* [18]. The traditional bicoherence [23] construction, however, has certain limitations that can often result in misidentification of phase-coupled noise disturbances. To rectify it, we introduce the phase-randomized (PR) bicoherence analysis to GW data, and demonstrate its utility with simulated signal studies in Sec. 2. In practice, random noise can sometimes mimic the bicoherence response of phase-coupled (PC) disturbances, thereby leading to false detections, or false alarms, even when phase randomization is used. To determine whether there is evidence of phase-coupling in the data or not, a hypothesis test is carried out between PC and non-phase-coupled (NPC) disturbances by employing the PR bicoherence analysis. Along the way, we derive an expression for the bicoherence value that minimizes the false identification of non-phase-coupled disturbances as phase-coupled ones in Sec. 3. This is useful for assessing how significant any phase-coupled disturbance is based on its bicoherence value. In Sec. 4, we apply the PR bicoherence analysis to GW data from LIGO detectors, and the utility of this analysis to identify nonlinear couplings is explained in terms of three examples in real data.

2. Higher order statistics – Quadratic Phase Coupling

Higher-order statistics, such as the bicoherence at the 3^{rd} order, can be helpful in identifying the presence of nonlinear frequency and phase couplings in the data [18].

The frequencies of different disturbances can nonlinearly combine to produce excess noise at other frequencies. The simplest and often the most dominant term in nonlinear couplings is the quadratic term, which results in the Quadratic Phase Coupling (QPC) [24]. Take, e.g., a pair of disturbances or “signals”, $x(t)$ and $y(t)$, that quadratically couple to form a new signal. Here we will be typically interested in a third time-series, $z(t)$, that is significantly influenced by that quadratic coupling, namely,

$$z(t) = p [x(t) + y(t)]^2 + q [x(t) + y(t)] + C(t), \quad (1)$$

where p and q are real numbers, and $C(t)$ is the noise. When $p = 0$, one has $x(t)$ and $y(t)$ affecting $z(t)$ at most linearly. In such a case, the influence of $x(t)$ or $y(t)$ on $z(t)$ can be detected by computing the *coherence* of $x(t)$ or $y(t)$ with $z(t)$. However, when $p \neq 0$, the influence of $x(t)$ and $y(t)$ on $z(t)$ is nonlinear (quadratic, to be precise), and a third-order statistic, such as the bispectrum or bicoherence can be used to reveal this influence.

To compute the bicoherence statistic of these three time-series, we divide each of them into M concurrent segments, $x_\alpha(t)$, $y_\alpha(t)$ and $z_\alpha(t)$, respectively, where $\alpha = 1, \dots, M$ is the segment index. Their Fourier transforms are $\tilde{X}_\alpha(f)$, $\tilde{Y}_\alpha(f)$ and $\tilde{Z}_\alpha(f)$, respectively. In practice, we will take the latter three “functions” as discrete Fourier transforms and their arguments as discrete frequencies. In terms of those transforms, the *bispectrum* statistic is defined as

$$B(f_k, f_l) = \frac{1}{M} \sum_{\alpha=1}^M \tilde{X}_\alpha(f_k) \tilde{Y}_\alpha(f_l) \tilde{Z}_\alpha^*(f_m), \quad (2)$$

where f_k , f_l , f_m are taken to be discrete frequencies, with k and $l = 1, \dots, N$, $k \neq l$, and $f_m = f_k \pm f_l$, such that $m \leq N$. Here, N is the Nyquist frequency index and f_N will denote the Nyquist frequency. Thus, the above frequencies obey the properties: (i) $0 \leq f_{k,l} \leq f_N$; (ii) $0 \leq f_k \pm f_l \leq f_N$. The bispectrum is computed for pairs of frequencies (f_k, f_l) – also called *bifrequencies* – and obeys the following properties: (i) $B(f_k, f_l) = B^*(-f_k, -f_l) = B(f_l, f_k)$; and (ii) $B(f_k, f_l) = B(f_k, -f_k - f_l)$ [25]. If \tilde{Z} has a signal that is phase-coupled with $\tilde{X}(f_k)$ and $\tilde{Y}(f_l)$, then the bispectrum can assume large values at the bifrequency (f_k, f_l) if that coupling is strong. A normalized version of the bispectrum is defined as:

$$b(f_k, f_l) = \frac{|B(f_k, f_l)|}{\sqrt{E[|\tilde{X}(f_k) \tilde{Y}(f_l)|^2] E[|\tilde{Z}(f_m)|^2]}}, \quad (3)$$

and is called the *bicoherence* [26]. Here, $|\tilde{A}(f_l)|^2 \equiv \tilde{A}_\alpha(f_l) \tilde{A}_\alpha^*(f_l)$ and $E[\tilde{A}(f_l)] \equiv \frac{1}{M} \sum_{\alpha=1}^M \tilde{A}_\alpha(f_l)$. Below, we will most often employ the bicoherence instead of the bispectrum.

In the context of GW data analysis, $x(t)$, $y(t)$ and $z(t)$ are time-series data from the GW strain channel or any of the auxiliary GW detector channels (e.g., associated with instruments and sensors). When one sets $x(t) = y(t) = z(t)$ in Eq. (3), the resulting statistic is called the *auto-bicoherence*. Otherwise the statistic is also called the *cross-bicoherence*. In this work, we focus on the auto-bicoherence and briefly present a feasibility study on the cross-bicoherence in Appendix C.

The bispectrum is manifestly complex and its phase is called the *biphase*, Φ_d . If $\Phi(f_k)$, $\Phi(f_l)$, and $\Phi(f_m)$ denote the phases of $\tilde{X}_\alpha(f_k)$, $\tilde{Y}_\alpha(f_l)$ and $\tilde{Z}_\alpha(f_m)$, respectively, then $\Phi_d \equiv \Phi(f_k) + \Phi(f_l) - \Phi(f_m)$. The utility of the variance of the biphase will be discussed in the following section, and is denoted as $\sigma'_\Phi{}^2$. It is empirically related to the bicoherence [27] as

$$\sigma'_\Phi{}^2 \approx \frac{1}{2M} \left[\frac{1}{b^2(f_k, f_l)} - 1 \right]. \quad (4)$$

Given a bifrequency, if the corresponding biphases of the M segments happen to be independent of one another, and have a uniform distribution in the interval $(-\pi, \pi]$, then its bispectrum ≈ 0 . Its bicoherence will be negligible as well. On the other hand, any bifrequency with a zero biphase will result in a non-vanishing bispectrum, and a bicoherence ≈ 1 .

Unfortunately, the bicoherence – as *traditionally* defined in Eq. (3) – suffers from the limitation that it can turn out to be unity even when there is no phase coupling. This can happen, e.g., when Φ_d is a constant across all M segments. In that event, the bicoherence is just $|E[e^{i\Phi_d}]| = |e^{i\Phi_d}|$, which is unity. This would be a false alarm since that value is indistinguishable from the one expected of a phase-coupled signal, where the biphase is 0 and, consequently, the bicoherence is unity. One way to address this problem is to multiply the phase Φ_d^α of the data from each segment with a random variable $R^{(\alpha)}$ such that $R^{(\alpha)}$ is the α -th realization of a random variable that follows either a uniform distribution over $(-\pi, \pi]$ or a zero-mean normal distribution with a variance σ_R^2 . The phase-randomized bispectrum is:

$$B_{\text{pr}}(f_k, f_l) = \frac{1}{M} \sum_{\alpha=1}^M |\tilde{X}_\alpha(f_k) \tilde{Y}_\alpha(f_l) \tilde{Z}_\alpha^*(f_m)| e^{iR^{(\alpha)}\Phi_d^\alpha}, \quad (5)$$

and the *phase-randomized* bicoherence $b_{\text{pr}}(f_k, f_l)$ is given by Eq. (3) with $B(f_k, f_l)$ replaced by $B_{\text{pr}}(f_k, f_l)$. The PR prescription works equally well regardless of which of the two distributions is used for R^α [25]. The expression for the variance of biphase corresponding to phase-randomized bicoherence is similar to Eq. (4). It is estimated by using $b_{\text{pr}}(f_k, f_l)$ instead of $b(f_k, f_l)$, and the variance of its biphase will be denoted as σ_Φ^2 .

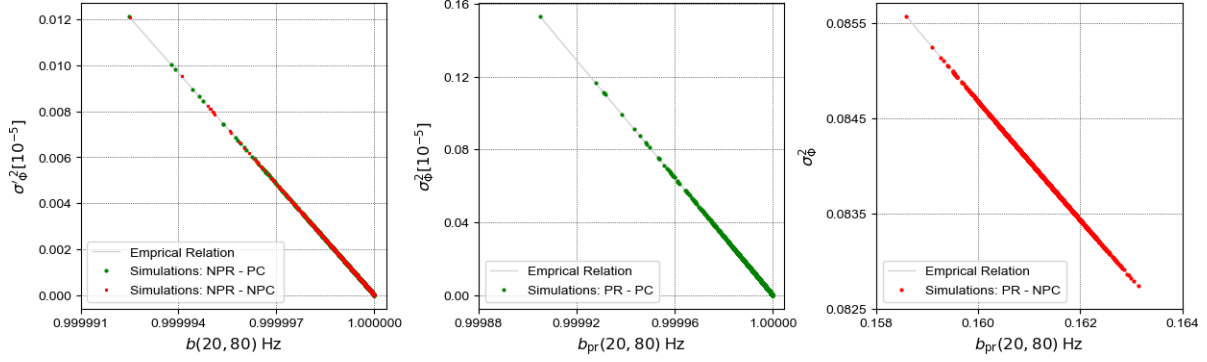


Figure 1: The impact of phase randomization on distinguishing nonlinearly phase-coupled signals (labeled “PC” and shown as green dots) from those without (labeled “NPC” and shown as red dots), in plots of biphase variance *vs* bicoherence. We compute these statistics for the (20,80) Hz bifrequency of the simulated PC and NPC signals described by Eq. (7). Each dot represents a different realization of the noise to which those signals are added. *Left*: Here the bicoherence is computed traditionally, i.e., with no phase randomization (NPR). Many PC signals show up with strong bicoherence values in this plot, but so do many NPC signals. The assumption that the bispectrum phases of the M segments are independent of one another is invalid for these NPC signals and leads to their high bicoherence values, thus, making it difficult to distinguish them from the PC signals. *Middle*: The bicoherence values of the PC signals shown in the left figure are minimally affected by the introduction of artificial phase randomization (PR). *Right*: For the same NPC signals shown in the left figure, the use of phase randomization helps in identifying the lack of phase coupling in those cases and gets their bicoherence to stay low. (The corresponding biphase variance tends to rise.) This helps in distinguishing the NPC signals from the PC ones when phase randomization is applied.

The strength of the phase couplings in a signal at any particular bifrequency, $b_{\text{pr}}(f_k, f_l)$, is inferred from the bicoherence value, which lies between 0 and 1. A true nonlinearly coupled bifrequency has $b_{\text{pr}}(f_k, f_l) \approx 1$. For non-phase coupled bifrequencies, one has $b_{\text{pr}}(f_k, f_l)$ closer to zero, for large enough M and when the noise in those segments is statistically independent.

Below we show with simulations how the bicoherence statistic can be used to discern the presence of quadratic phase coupling. Thereafter, we present some applications in real GW data. Throughout this paper, we fixed the values of some of the analysis parameters for both simulated signals and GW data, unless stated otherwise. The duration of all data chunks analyzed is chosen to be 4 sec, with a sampling frequency $f_s = 1024$ Hz; of course, the Nyquist frequency is set to $f_N = \frac{f_s}{2}$. For computing the bicoherence, each time-series data chunk is divided into M segments and their Fourier transforms taken after applying the Hanning window on them. We also use 98% overlap among consecutive segments.

The optimal choice for the number of segments (M) is decided empirically. For a fixed chunk duration, if M is small, then the relative contribution of noise to the bicoherence magnitude can be large. On the other hand, if M is large, then the overlap of the segments will be large for the same chunk duration. In such a case, the different segments will cease to be independent and the bicoherence for a real signal, of a similar duration as the chunk, will plateau. By performing injection of simulated signals in real data and studying known short duration couplings (lasting no more than a few seconds) we found $M \approx 31$.

2.1. Usefulness of the bicoherence: An example

We now setup a simulation of phase-coupled signals to demonstrate how the bicoherence can be used to detect that coupling. Consider the sinusoidal signals $x(t) = a_x \cos(2\pi f_x t + \Phi_x)$ and $y(t) = a_y \cos(2\pi f_y t + \Phi_y)$, with $a_{x,y}$, $f_{x,y}$ and $\Phi_{x,y}$ as the respective amplitudes, frequencies, and phases. Using these signals in Eq. (1), and setting $q = 0$ and $C(t) = n(t) - p(a_x^2 + a_y^2)/2$ there, we get:

$$z(t) = p [a_x \cos(2\pi f_x t + \Phi_x) + a_y \cos(2\pi f_y t + \Phi_y)]^2 + n(t) - p \frac{(a_x^2 + a_y^2)}{2}, \quad (6)$$

where $n(t)$ is Gaussian noise with a vanishing mean. Expanding Eq. (6) by using trigonometric identities, the signal takes the form

$$z(t) = p \left[\frac{a_x^2}{2} \cos(4\pi f_x t + 2\Phi_x) \right] + p \left[\frac{a_y^2}{2} \cos(4\pi f_y t + 2\Phi_y) \right] + p [a_x a_y \{ \cos(2\pi f_{zp} t + \Phi_{zp}) + \cos(2\pi f_{zn} t + \Phi_{zn}) \}] + n(t), \quad (7)$$

where $f_{zp} \equiv (f_x + f_y)$, $f_{zn} \equiv (f_x - f_y)$, $\Phi_{zp} \equiv \Phi_x + \Phi_y$ and $\Phi_{zn} \equiv \Phi_x - \Phi_y$.

In our simulations we constructed two kinds of signals: (a) A phase-coupled (PC) signal, modelled after $z(t)$, where Φ_{zp} and Φ_{zn} obey the preceding relations with Φ_x and Φ_y ; (b) A non-phase-coupled (NPC) signal, which is simulated similar to $z(t)$, except that it has $\Phi_{zp} \neq \Phi_x + \Phi_y$ and $\Phi_{zn} \neq \Phi_x - \Phi_y$. In fact, we chose the input parameter values in the simulated signals such that $f_x = 40$ Hz, $f_y = 60$ Hz, $\Phi_x = 40^\circ$, $\Phi_y = 60^\circ$, and $a_x = a_y = \sqrt{2}$. Also, the standard deviation of $n(t)$ was taken to be much smaller than $p (= 1)$ and was, in fact, set to 0.0025. For the PC signal, $f_{zp} = 100$ Hz, $f_{zn} = -20$ Hz, $\Phi_{zp} = 100^\circ$ and $\Phi_{zn} = -20^\circ$. Whereas for the NPC signal, all parameters were set to the same values as the PC signal except that $\Phi_{zp} = 0 = \Phi_{zn}$.

If one were to compute the cross-bicoherence of $x(t)$, $y(t)$, and $z(t)$, then one can expect high bicoherence values at the bifrequency of (40, 60) Hz, since signals at these frequencies are present in x and y , respectively, and the sum and difference (actually the absolute value of the difference) of those frequencies, namely, 100 Hz and 20 Hz, are represented in z as f_{zp} and f_{zn} , respectively.

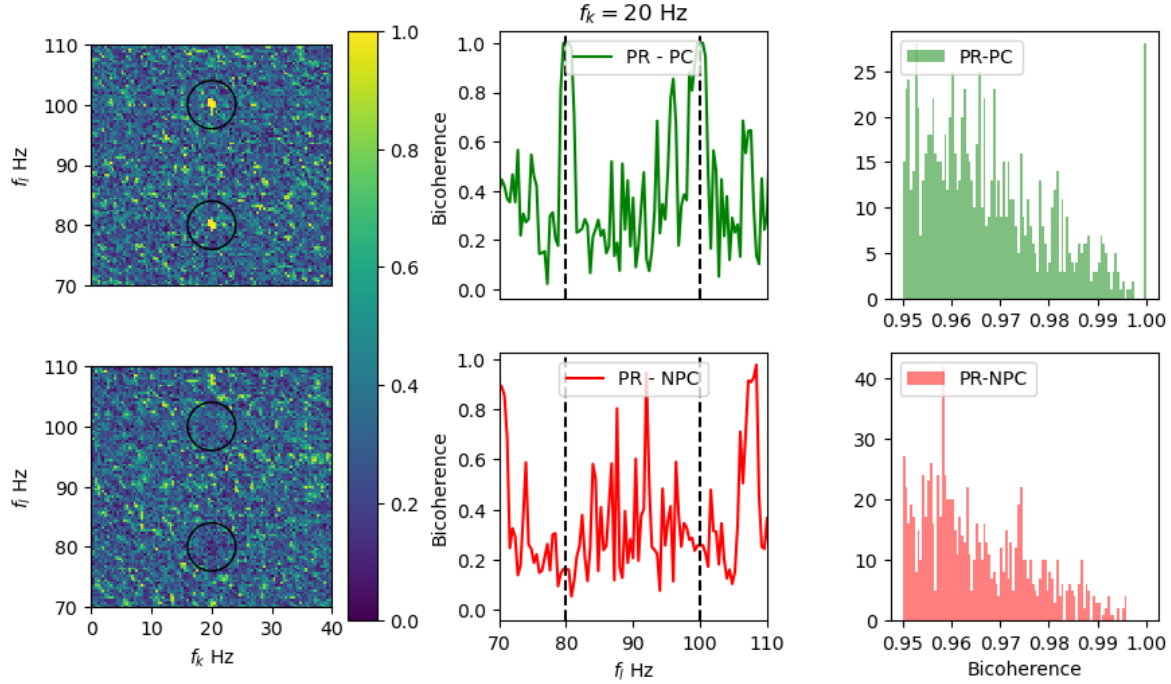


Figure 2: The two circles in the top-left bicoherence map mark the two phase-coupled (PC) bifrequencies, namely, (20,80) Hz and (20,100) Hz, corresponding to the signal in Eq. (7), with bicoherence of $\simeq 1$. Contrastingly, in the bottom-left bicoherence map of the corresponding NPC signal, the same region shows a bicoherence of $\simeq 0$, implying lack of phase coupling. Phase randomization (PR), which was used here, improves the identification of PC bifrequencies. To analyze the behavior of bicoherence at and around the bifrequencies (20,80) Hz and (20,100) Hz, line plots are shown in the middle two panels, with $f_l \in [70 - 110]$ Hz and f_k kept fixed at 20 Hz. The vertical dashed black lines correspond to the bifrequencies (20,80) Hz and (20,100) Hz. Top-middle: At the phase-coupled bifrequencies, the bicoherence is close to one. The bicoherence at those bifrequencies dips to low values for the non-phase-coupled case (bottom-middle plot). Note that for this (NPC) case, we chose $\Phi_{zp} = 0 = \Phi_{zn}$. The right panel shows the bicoherence histogram of the left panel. The bottom-right figure shows that the probability of misclassifying an NPC as PC signal is 11.76% for $b_{pr} > 0.995$, but drops to 0% above a value of $b_{pr} = 0.996$ (in this experiment).

However, when computing the auto-bicoherence of z , note that the four frequencies present in it are $2f_x = 80$ Hz, $2f_y = 120$ Hz, $|f_{zn}| = 20$ Hz and $f_{zp} = 100$ Hz. The only independent bifrequencies chosen from this set whose sum(s) or difference(s) can be found in the same set are (20,80) Hz (since 100 Hz is present in the same set) and (20,100) Hz (since 120 Hz is also present in the same set). This is, of course, expected, given the origin of z in x and y . (Note that the “reflected” pairs (80,20) Hz and (100,20) Hz will also have strong bicoherence values but are not independent of the above pairs, as described in Appendix A.)

To test the above expectations through simulations, we added the PC and NPC versions of $z(t)$, separately, into 2000 realizations of noise, $n(t)$. For these simulated data sets, for PC and NPC cases, we then computed the (auto-)bicoherence values and their corresponding biphasic variances without applying phase randomization. We repeated the experiment after applying phase randomization, and plotted results from both studies in Fig. 1, which shows that phase randomization improves the distinguishability of phase-coupled signals from non-phase-coupled signals.

The bicoherence maps of the same simulated signals, for the PC and NPC cases, are shown in Fig. 2 (left panel). The right panel in Fig. 2 is the non-redundant [†] bifrequencies histogram. The middle panel shows the values of b_{pr} as a function of f_l when f_k is held fixed at 20 Hz. The bottom-right figure shows that the probability of misclassifying an NPC as PC signal is 11.76% when the bicoherence (b_{pr}) threshold is set to 0.995, but drops to 0% for $b_{\text{pr}} > 0.996$ (in this experiment). The non-linear phase couplings in the signal are identified correctly through the phase randomized bicoherence method. In this paper, the bicoherence maps are positive quadrants of the bicoherence plane (see Appendix A). Note that each octant in the bicoherence plane captures complete information about the bifrequencies owing to its eight-fold symmetry.

3. Estimating detection threshold

In the previous section, we demonstrated that applying phase randomization in the computation of bicoherence improves the distinguishability of PC and NPC cases. This improvement rests on the following reasonable assumptions about the signals: (i) the phase component of bifrequencies Φ_k^α and Φ_l^α are uniformly distributed random variables, over $(-\pi, \pi]$; (ii.a) For the NPC bifrequencies, we shall take that $\Phi_m^\alpha \neq 0 \neq \Phi_d^\alpha$; (ii.b) For NPC cases, Φ_m^α and Φ_d^α are uniformly distributed as $\sim U(-\pi, \pi]$ [25] and independent of Φ_k^α and Φ_l^α ; (iii) For the PC bifrequencies, $\Phi_d = 0$ – although, in practice, it is not exactly zero and can be assumed to have a normal distribution, i.e., $\Phi_d \sim N(0, \sigma_\Phi^2)$ [27]. However, the true phase-coupled bifrequencies can become indistinguishable from noise when the signal's power or the strength of the phase coupling is low. This can lead to a false dismissal of PC. Therefore, a test is required to decide whether or not there is phase coupling present at any bifrequency. We assume two hypotheses that are tested on the simulated data:

$$\begin{aligned} \text{Null hypothesis, } H_0 : \text{ NPC, } \Phi_d &\sim U(-\pi, \pi], \quad b_{\text{pr}}^2(f_k, f_l) \approx 0. \\ \text{Alternative hypothesis, } H_1 : \text{ PC, } \Phi_d &\sim N(0, \sigma_\Phi^2), \quad b_{\text{pr}}^2(f_k, f_l) \approx 1. \end{aligned}$$

We define T as the detection threshold for bicoherence. The two types of errors associated with these hypotheses and the choice of T that we are interested in are

[†] See Appendix A.

the false-positive and false-negative errors [25]. Suppose in reality there is no phase-coupled signal in the data. In such a case, finding $b_{\text{pr}}^2(f_k, f_l) > T$ implies a false detection of PC. This is a false-positive error and its probability of occurrence is:

$$\begin{aligned} P_{\text{fp}} &= P \{H_1 \mid H_0\} \\ &= P \left\{ b_{\text{pr}}^2(f_k, f_l) > T \mid \text{NPC} \right\}. \end{aligned} \quad (8)$$

Using Eq. (5) one can show that the phase randomized bicoherence obeys $b_{\text{pr}}^2(f_k, f_l) = e^{-\sigma_{\text{R}}^2 \Phi_{\text{d}}^2}$, where the randomization variable R^α for every segment was chosen to be distributed as $N(0, \sigma_{\text{R}}^2)$ for mathematical convenience [25]. Then, Eq. (8) becomes

$$\begin{aligned} P_{\text{fp}} &= P \left\{ e^{-\sigma_{\text{R}}^2 \Phi_{\text{d}}^2} > T \mid \Phi_{\text{d}} \sim U(-\pi, \pi) \right\} \\ &= P \left\{ |\Phi_{\text{d}}| < \frac{\sqrt{\ln \frac{1}{T}}}{\sigma_{\text{R}}} \mid \Phi_{\text{d}} \sim U(-\pi, \pi) \right\} \\ &= \frac{\sqrt{\ln \frac{1}{T}}}{\pi \sigma_{\text{R}}}, \end{aligned} \quad (9)$$

which shows that as T increase the probability of false-positives decreases. On the other hand, when the phase-coupled bifrequency has bicoherence value less than the threshold value, i.e., $b_{\text{pr}}^2(f_k, f_l) \leq T$, one has a case of false rejection of PC. The probability of occurrence of such false-negatives is

$$\begin{aligned} P_{\text{fn}} &= P \{H_0 \mid H_1\} \\ &= P \left\{ b_{\text{pr}}^2(f_k, f_l) \leq T \mid \text{PC} \right\}. \end{aligned} \quad (10)$$

As discussed before, in practical cases of PC signals, one has $\Phi_{\text{d}} \approx 0$, with a small variance. In fact, it is normally distributed as $\approx N(0, \sigma_{\Phi}^2)$, with σ_{Φ} characterizing the phase coupling [27]. With this input, Eq. (10) becomes

$$\begin{aligned} P_{\text{fn}} &= P \left\{ e^{-\sigma_{\text{R}}^2 \Phi_{\text{d}}^2} \leq T \mid \Phi_{\text{d}} \sim N(0, \sigma_{\Phi}^2) \right\} \\ &= P \left\{ |\Phi_{\text{d}}| \geq \frac{\sqrt{\ln \frac{1}{T}}}{\sigma_{\text{R}}} \mid \Phi_{\text{d}} \sim N(0, \sigma_{\Phi}^2) \right\} \\ &= 2 \int_{\lambda}^{\infty} N e^{-\frac{\Phi_{\text{d}}^2}{2\sigma_{\Phi}^2}} d\Phi_{\text{d}}, \end{aligned} \quad (11)$$

where $\lambda = \frac{\sqrt{\ln \frac{1}{T}}}{\sigma_R}$ and $N = \frac{1}{\sqrt{2\pi}\sigma_\Phi}$.

The bicoherence value, T_{\min} , that minimizes the probability of detection error, $P_E = P_{\text{fp}} + P_{\text{fn}}$, can be estimated by differentiating P_E with respect to T [25]; it is found to be:

$$T_{\min} = \left(\frac{\sigma_\Phi}{\sqrt{2\pi}} \right)^{2\sigma_\Phi^2 \sigma_R^2}. \quad (12)$$

Typically, T_{\min} is set as the lower limit of the phase-randomized bicoherence for identifying cases of phase-coupled signals. Substituting T_{\min} in Eqs. (9) and (10), we get P_{fp} and P_{fn} , which now depend on σ_Φ alone. Indeed, P_{fp} can be expressed as

$$P_{\text{fp}} = \frac{\sigma_\Phi}{\pi} \sqrt{\ln \left(\frac{2\pi}{\sigma_\Phi^2} \right)}. \quad (13)$$

The expression for the corresponding P_{fn} remains the one in Eq. (11), with the lower limit of that integration now set to $\lambda = \sigma_\Phi \sqrt{\ln \left(\frac{2\pi}{\sigma_\Phi^2} \right)}$. The P_{fp} and P_{fn} corresponding to T_{\min} present the advantage that they can be estimated directly from the variance of the biphas, and are cheaper to compute in practice.

The two hypotheses were tested on the simulated data sets. One can anticipate that the bicoherence value of PR–PC is closer to one, whereas PR–NPC is closer to zero. This anticipation is true in NPC and PC distributions of simulated signals at $b_{\text{pr}}(20, 80)$ Hz, as shown in Fig. 3. The shaded regions in both plots of Fig. 3 each correspond to a 95% confidence interval. These regions are well separated, and the probability of false-positive is low even for a high value of the bicoherence threshold. In real data applications below, we choose to be conservative in identifying phase-coupled signals, and set the threshold of the bicoherence b_{pr} to be high, *viz.* $b_{\text{pr}} = 0.98$. The false-alarm probability at such high values is quite low, as evidenced in Fig. 1. ‡ Consequently, we analyze only the most significant cases of suspected PCs. As we make advances in developing more computationally efficient algorithms for computing bicoherence, we will lower this threshold further.

4. Application to gravitational-wave data

In this section, we study applications of bicoherence for finding phase-coupled signals in real GW data. Certain disturbances in detector systems or their environment (e.g., due to scattered light or seismic vibrations) can sometimes introduce excess noise in the

‡ As we explain below, the false-alarm probability is further lowered owing to the fact that we apply a threshold on the strength of the transient non-Gaussian noise chosen for follow-up search for non-linear couplings.

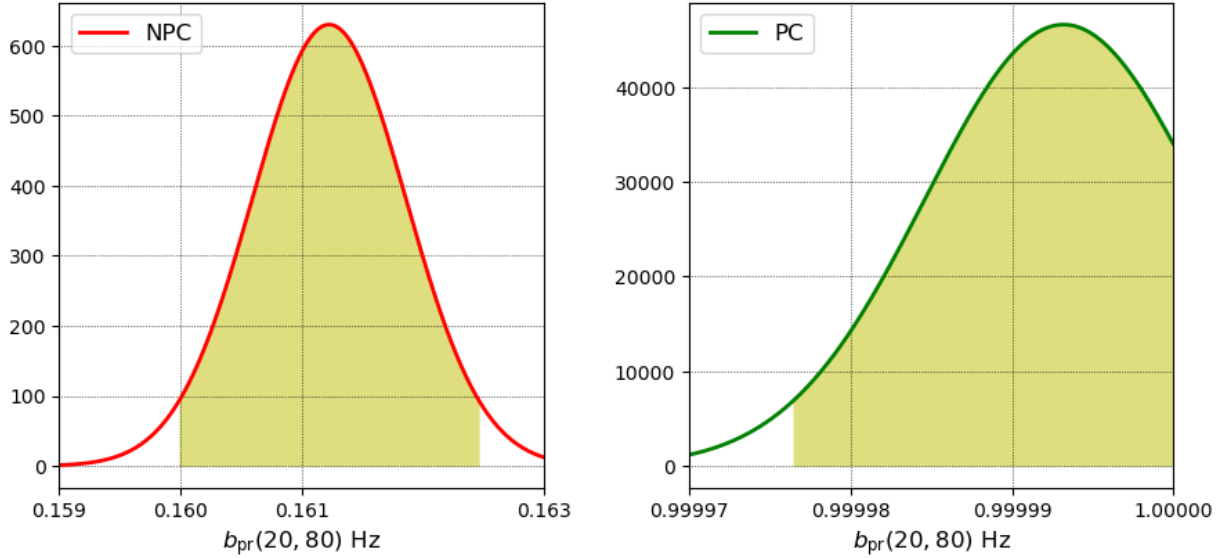


Figure 3: Distributions of the bicoherence values of the simulated non-phase coupled (NPC) signals (left) and the phase-coupled (PC) ones (right) described in Eq. (7), at the bifrequency (20,80) Hz. Each shaded region corresponds to a 95% confidence interval. These regions have very little overlap. Therefore, one can afford to set the bicoherence threshold to be quite high in this simulation, e.g., at $b_{pr} = 0.9999$, and benefit from a low false-negative probability while also enjoying a low false-positive probability.

detector strain and affect the quality of GW strain data. In this work, we are interested in disturbances that create transient non-Gaussian noise – also called *glitches*, which typically last for a few milliseconds to several seconds [28, 29]. Certain classes of glitches (e.g., blips) are known to trigger templates used for searching GW signals from compact binary coalescences (CBCs), thereby creating false alarms. The origin of several classes of glitches is not entirely known. Some others are known to originate through linear or non-linear coupling mechanisms among auxiliary channels [18, 19]. The auto-bicoherence can be an initial diagnostic tool for identifying potentially phase-coupled glitches in the GW strain data. This work focuses on such an analysis in open-source data [30].

Importantly, failing to apply artificial phase randomization in the computation of auto-bicoherence can lead to false detection of PC bifrequencies. Consequently, the bicoherence maps also show different patterns depending on whether PR is used or not. One of the blip glitches that occurred in a LIGO detector during the O2 observation run with high excess power is demonstrated in Figure 4, where the effect of PR can be clearly discerned. We continue to apply PR in all our bicoherence analysis below.

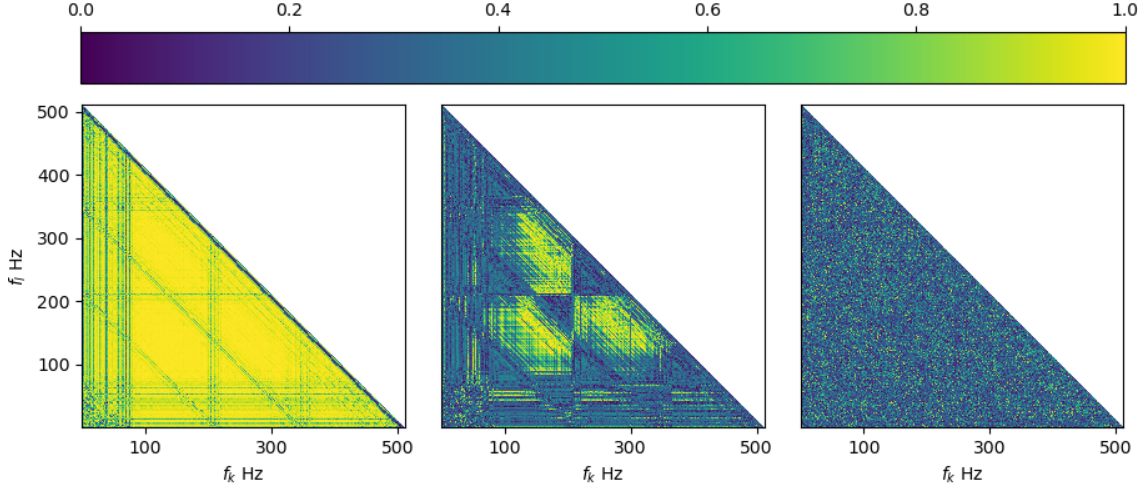


Figure 4: The bicoherence map of a blip glitch, constructed without phase randomization (PR), is shown on the left. The colorbar shows the bicoherence. It incorrectly shows many coupled bifrequencies, which disappear when the bicoherence is computed using phase randomization, as shown in the middle figure. This figure also reveals that the glitch may have been triggered from disturbances in frequencies that up-converted due to phase couplings. *Column-3*: For comparison, we show here the PR bicoherence map of the background noise data that does not contain any glitch. Such data show the absence of any significant phase coupling.

4.1. Using bicoherence to classify glitches

Instances of transient excess noise often show up in auxiliary channels and are detected by tools such as Omicron [31]. This tool performs a multi-resolution time-frequency analysis of detector data around such instances. Glitches with excess power above a given threshold are flagged for further inspection in data quality studies and astrophysical searches. Also, the time-frequency (TF) maps or spectrograms of Omicron serve to classify glitches via human intervention and machine learning [29, 32].

The blip glitches [33] form one of the categories of glitches. These are short noise transients that have a high-frequency bandwidth and often trigger CBC templates. In fact, it is the high-mass binary black hole search that is affected most by them. This is because these signals have a small number of wave-cycles in band and are of durations comparable to those glitches [11]. Blips appeared at the rate of approximately 4 per hour at Livingston (L1) and 2 per hour at Hanford (H1) during their third observation run (O3) [9]. Koi fish and Tomtes are two other classes of glitches. While their morphologies share some characteristics with blips, important distinctions exist (see, e.g., Refs. [33, 34, 35]). Extremely loud glitches [9] (with Omicron SNR > 100) are another class of glitches that adversely affect a detector’s sensitivity to searches of transient astrophysical signals. Studies have been carried out to identify the origin of these glitches, but no clear conclusion has been arrived at yet for several glitch types.

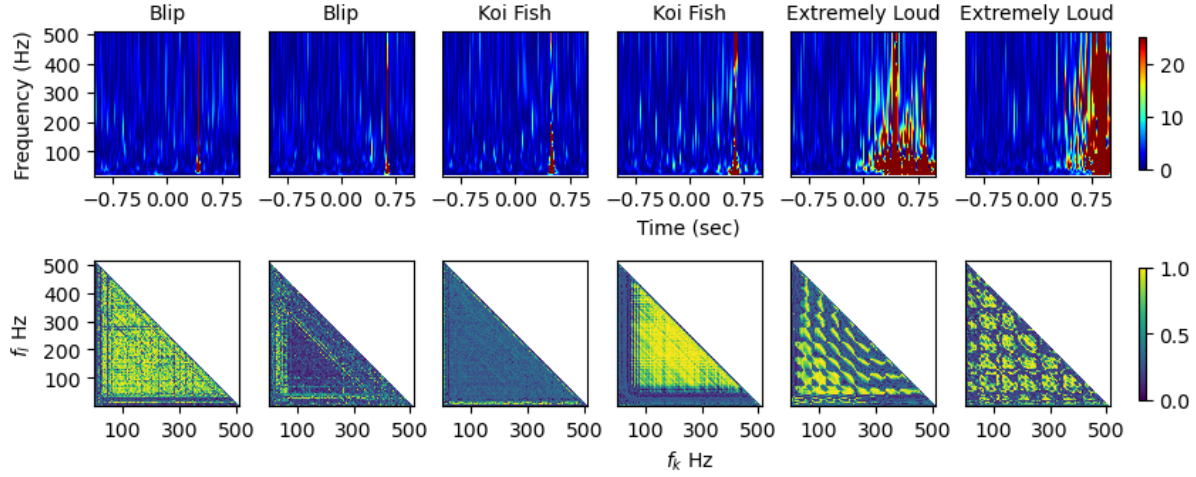


Figure 5: A comparison of second-order and third-order statistics of glitches. The top row shows the spectrograms of pairs of blips (columns 1-2), koi fish (columns 3-4) and “extremely loud” glitches (columns 5-6). The spectrograms look similar within each category, e.g., blips, simply because the glitches were categorized by the patterns revealed in those maps in the first place. They are different – to varying degrees – across categories, e.g., blips and extremely loud glitches. The bottom row shows the corresponding phase-randomized bicoherence maps, constructed using 4 sec data chunks centered at the glitches. Variations in the bicoherence maps within some glitch categories (e.g., columns 3 and 4 of koi fish) suggest the presence of different phase-coupled bifrequencies or a difference in the nature of that coupling. On the other hand, similarities in these maps across glitch categories (e.g., columns 1 and 4) suggest the presence of similar nonlinear phase couplings in different glitch types. Information in both types of maps, combined, can help in troubleshooting the origin of these noise artifacts.

The bicoherence maps of the blip, koi fish, and extremely loud glitches are produced by applying the phase-randomized auto-bicoherence analysis to look for 3rd-order similarities in each class. If the observed glitches have a common source, their bicoherence maps will have similarities owing to common bifrequencies related to that source. Such expectations have been borne out in the study of 2nd-order statistics, such as the TF maps of Omicron, as depicted in the upper panel of Fig. 5. The top row in that figure shows the spectrograms of pairs of blips (columns 1-2), koi fish (columns 3-4) and “extremely loud” glitches (columns 5-6). The spectrograms look similar within each category, e.g., blips, simply because the glitches were categorized by the patterns revealed in those maps. They are different – to varying degrees – across categories (e.g., blips and extremely loud glitches). The bottom row shows the corresponding phase-randomized bicoherence maps, constructed using 4sec data chunks centered at the glitches. Variations in the bicoherence maps within some glitch categories (e.g., columns 3 and 4 of koi fish) suggest the presence of different phase-

coupled bifrequencies or a difference in the nature of that coupling. On the other hand, similarities in these maps across glitch categories (e.g., columns 1 and 4) suggest the presence of similar nonlinear phase couplings in different glitch types. These maps indicate, e.g., that all blips are not made identically. In future, cross-bicoherence maps can help diagnose their origins by revealing what detector systems couple non-linearly to produce them.

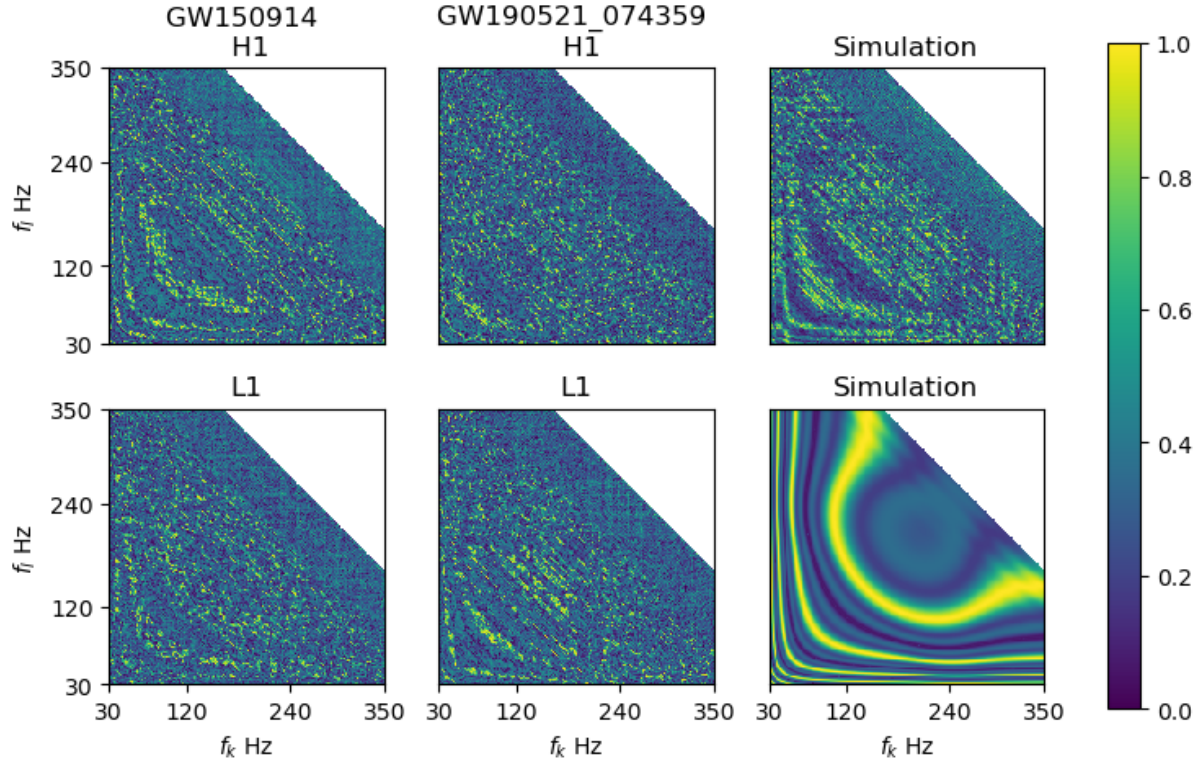


Figure 6: Phase-randomized bicoherence maps of the data from the binary black hole (BBH) signals GW150914 (column 1) and GW190521_074359 (column 2), as well as a simulated BBH signal (column 3). The bicoherence maps in the left and middle columns show interesting yet expected similarities between H1 and L1 signals. The top right figure shows such a map for a simulated GW150914-like signal added to detector noise, which itself is simulated using the noise power-spectral density of H1 data from around that event. The bottom right figure shows the same simulated GW150914-like signal but with no noise added. Note that the bicoherence patterns here are in themselves not evidence for the presence of phase coupling between detector systems at that time. Rather, these patterns are characteristic of binary waveforms. In identifying glitches by using their *auto*-bicoherence maps, it will be important to utilize this knowledge so as not to confuse real CBC signals for glitches.

It is also interesting to inquire if bicoherence maps can be used to distinguish between Compact Binary Coalescence (CBC) signals and glitches arising from non-linear couplings. We leave this question for a future work to investigate but provide

some preliminary findings here. By applying the PR auto-bicoherence analysis to GWTC-3 [7] catalog events we examine the apparent phase coherence in the data with CBC signals. We noticed significant phase coherence in a few GW events. Two of those, namely, GW events GW150914 [36], and GW190521_074359 [5] are presented in Fig. 6 along with a simulated signal for aiding the interpretation of their bicoherence maps. The presence of significant bicoherence is evident there. To prepare the GW strain data for the bicoherence analysis, first a high-pass filter is applied with cut-off frequency 20 Hz, followed by whitening and the application of a bandpass filter, from 30 to 350 Hz, with notches of the first three power line harmonics [37]. The noise power-spectral density (PSD) is estimated from 32 sec of data using the Welch method.

To ensure that the phase couplings revealed in GW events’ bicoherence maps are not from glitches, we modeled two signals similar to the GW150914 event, with and without strain noise. In Fig. 6 (row 1, column 3), the 8 second long time-series noise was simulated by using the H1 noise PSD available in Ref. [38] for the GW190514 event. A simulated CBC signal was added to that noise before producing the plot. On the other hand, in Fig. 6 (row 2, column 3) no noise was added to the CBC signal. The bicoherence patterns in the map of the modeled signal, with added simulated noise, resembles those of the GW150914 signal, as shown in Fig. 6 (row 1, column 3). These signals were produced from the SEOBNRv4_opt waveform [39], with component masses of $36 M_{\odot}$ and $30 M_{\odot}$. This family of waveforms was constructed in the literature by calibrating effective one-body waveforms with an extensive set of numerical relativity waveforms, and have been employed in LIGO-Virgo CBC searches (see, e.g., Ref. [40]). The matched-filter SNR of the signal is 20. At the very least, the knowledge of these bicoherence patterns will be important in not confusing real CBC signals for noise artifacts and, therefore, for the purpose of veto safety.

4.2. Recurrent bifrequencies in the quieter Omicron triggers

In this subsection, we report on results from the PR auto-bicoherence analysis performed to identify repeated phase-coupled bifrequencies in the relatively quiet Omicron triggers in O3. These triggers have received inadequate attention [41] and can be detrimental to the quality of GW data. Every quiet omicron trigger chosen for bicoherence analysis here satisfies two conditions: (1) The Omicron SNR lies in the narrow range $[5, 5.001]$; (2) No other Omicron trigger exists within ± 3 sec duration of the trigger time of interest. Based on these criteria, we selected the triggers shown in Fig. 7.

Observation Run	Hanford (H1)	Livingston (L1)
O2	751	534
O3	1079	440

Table 1: The number of “quiet” Omicron triggers considered here for identifying recurrent bifrequencies in the O2 and O3 observation runs.

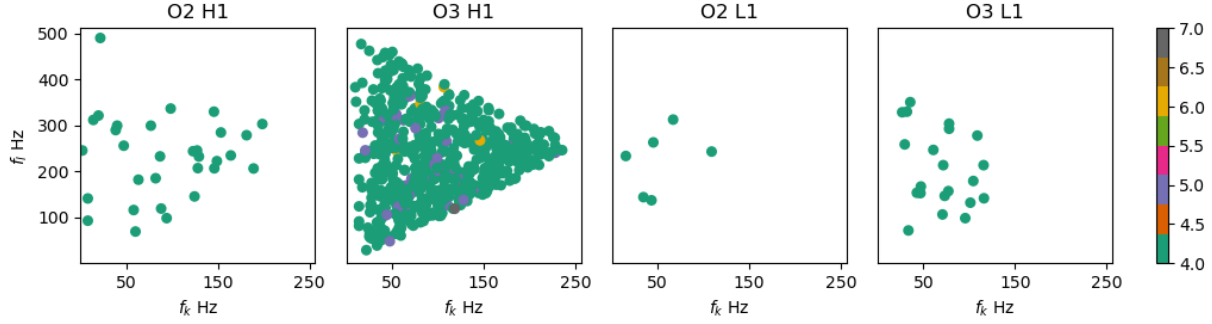


Figure 7: Recurrent bifrequencies with $b_{pr} \geq 0.98$ among the quieter Omicron triggers. When triggers with the same bifrequency occur more than three times during a run, we record them. These bifrequencies, from the second and third observation runs of H1 and L1 detectors, are shown here. The colorbar represents the number of such occurrences.

In Fig. 7, we plot the bifrequencies of those quiet triggers that have $b_{pr} \geq 0.98$. This value is somewhat less than the bicoherence threshold discussed for simulations in earlier sections but not too small to increase the false-positive rate significantly. When the same PC bifrequencies are found in more than three quiet triggers in the same detector, then that type of coupling is noted here as significant. These select bifrequencies, from the O2 and O3 observation runs of L1 and H1 detectors, are displayed in Fig. 7. To probe possible causal connections with known noisy instances, the sum of the frequencies in each bifrequency pair in this shortlist is compared with the frequencies of gated lines [42, 43, 44, 45] in those observation runs. § When that comparison reveals a match, an instance of non-linear coupling can be suspected. The closest matches are reported in Table 2. This comparison does not reveal any significant match in the L1 detector. The H1 detector, however, shows some interesting cases that merit further study to establish causal connections. While the auto-bicoherence does not establish, on its own, the presence of nonlinear frequency couplings or their cause, it does help in narrowing down the broad sensitivity band of the detectors to a manageably short list of frequencies that can be followed-up with additional analysis, such as an examination of auxiliary channels with the *cross-bicoherence*, for that purpose.

We also report that the nonlinear couplings between the mechanical resonances of test masses reported in our earlier work [18] are found to exist in more recent observation runs as well. Specifically, the bounce and the violin modes of test masses (which register in the bicoherence map at bifrequency (10, 495.2) Hz) as well as the power line harmonics and their sub-harmonics identified in that analysis can be found in O3 too.

§ Differences of frequencies in some bicoherence triggers have also been found to be associated with gated lines but are not listed here, even though investigation continues on the origin of those features.

Bifrequency $b_{\text{pr}}(f_k, f_l)$ Hz	Bifrequency sum (Hz)	Gated lines (Hz)	Gated lines Comments
O2 H1			
198.4, 303.2	501.6	501.61	Violin mode 1st harmonic ITMY Mode 1
		501.68	Violin mode 1st harmonic ITMY Mode 2
O3 H1			
10.0, 383.2	393.2	393.2	Calibration line non-linearity
16.4, 477.2	493.6	493.61514 493.62598 493.62653	Likely calibration line mixing
30.0, 54.4	84.4	84.4	Calibration line non-linearity
38.0, 66.4	104.4	104.4	
40.0, 448.8	488.8	488.78625	Likely calibration line mixing
48.8, 250.8	299.6	299.6	Beam splitter violin mode region
55.2, 244.4			
68.4, 420.4	488.8	488.78625	Likely calibration line mixing
78.0, 423.6	501.6	501.63223 501.69513	Violin mode 1st harmonic
134.0, 337.6	471.6	471.68625	Likely calibration line mixing
150.8, 242.4	393.2	393.2	Calibration line non-linearity
155.6, 333.2	488.6	488.78625	Likely calibration line mixing
206.0, 282.4	488.4	488.48624	
221.2, 287.6	508.8	508.84515	Violin mode 1st harmonic

Table 2: A list of bifrequencies with $b_{\text{pr}} \geq 0.98$. The sum of the two frequencies in a significant bifrequency pair is compared with the frequency of the gated lines in the O2 and O3 observation runs. The closest match of those frequencies is reported here (in H1). No such match was found in L1 at the same level of significance.

5. Conclusion

We demonstrated how third-order statistics, in the form of the bicoherence and biphas, are useful in revealing noise transients with instances of nonlinear couplings among various components of a detector. While for some transients the offending contributors to such couplings were identified here, nevertheless more work will be needed in the future to improve the fraction of successful identifications and establish terrestrial causes.

It is important to stress that introducing artificial phase randomization in analyzing the data does not affect the actual phase coupling in the signal, but reduces the false detection of such couplings. We demonstrated this with simulations as well as an example of a glitch that appeared in real GW data. We used the PR auto-bicoherence to examine the similarities and differences in the phase-coupled frequencies within certain categories of glitches as well as across them. This third-order statistic provides an additional way of characterizing glitches than Omicron spectrograms and may

contribute to troubleshooting their origins and subsequent removal or mitigation. It is also important to realize that the bicoherence tool developed here is not limited to characterizing glitches and can identify other features in GW data, such as the interesting frequency evolution of CBC signals, even though this is not its primary objective. We demonstrated this with a couple of examples of actual GW events and simulated signals as proof of concept.

In future, we plan to study the cross-bicoherences of multiple auxiliary channels at the time of glitches. This will aid in identifying if nonlinear coupling of any of those channels are involved in producing the glitch. While conceptually its computation is not very different from that of auto-bicoherence, nevertheless sieving through dozens of auxiliary channel pairs significantly increases the computation load. New algorithms for computing it are being explored to find ways of reducing this load.

A note on software used and developed

We developed a customized Python [46] based Bicoherence (PyBicoh) analysis package for deployment in GW strain data [47]. It was used for producing the various auto-bicoherence maps and results discussed in this paper. We used GwPy [48] to fetch and read GW data. PyCBC [49] functions were used to simulate CBC waveforms and detector noise time-series (from a specified noise PSD). All the figures in this paper are plotted with matplotlib [50], with support from scipy [51], numpy [52], astropy [53], and h5py [54].

Acknowledgements

We thank Andrew Lundgren, Fred Raab, Jess McIver, Robert Bruntz, T. R. Saravanan, Shivaraj Kandhasamy, Suresh Doravari, Sanjit Mitra, Siddharth Soni, and Sunil Choudhary for discussions. Thanks are due to Miriam Cabero for discussions on blip glitches. Deepak Bankar and Malathi Deenadayalan provided valuable computing-cluster support. We thank Ronaldas Macas for carefully reading the manuscript and sharing his comments on it. SS would like to thank Michał Bejger and acknowledge support provided by Tata Trusts and LIGO-India grants at IUCAA and NCN-OPUS grant 2021/43/B/ST9/01714. We are also grateful for the support provided by the Sarathi computing cluster (IUCAA) and the computational resources provided by the LIGO Laboratory supported by National Science Foundation Grants PHY-0757058 and PHY-0823459. This material is based upon work supported by NSF's LIGO Laboratory, a major facility fully funded by the National Science Foundation. We also acknowledge support from the NSF under grant PHY-2309352.

Appendix A. The bicoherence plane

In Fig. A1, the part of the plane enclosed by the hexagon $ABCDEF$ is a valid bicoherence analysis section. Sections of quadrant 1 of this plane are considered for the bicoherence analysis in this work and displayed in our bicoherence maps. The region $\triangle OPA$ (green borders) is the principal region of non-redundant bispectral information. Other regions, such as $\triangle OPB$ (magenta borders), have the same information. Specifically, patterns in $\triangle OPB$ of a bicoherence map will be identical to those in $\triangle OPA$ but with reflection on the line OP . Note that the frequencies in these regions are confined within the Nyquist frequency (f_N).

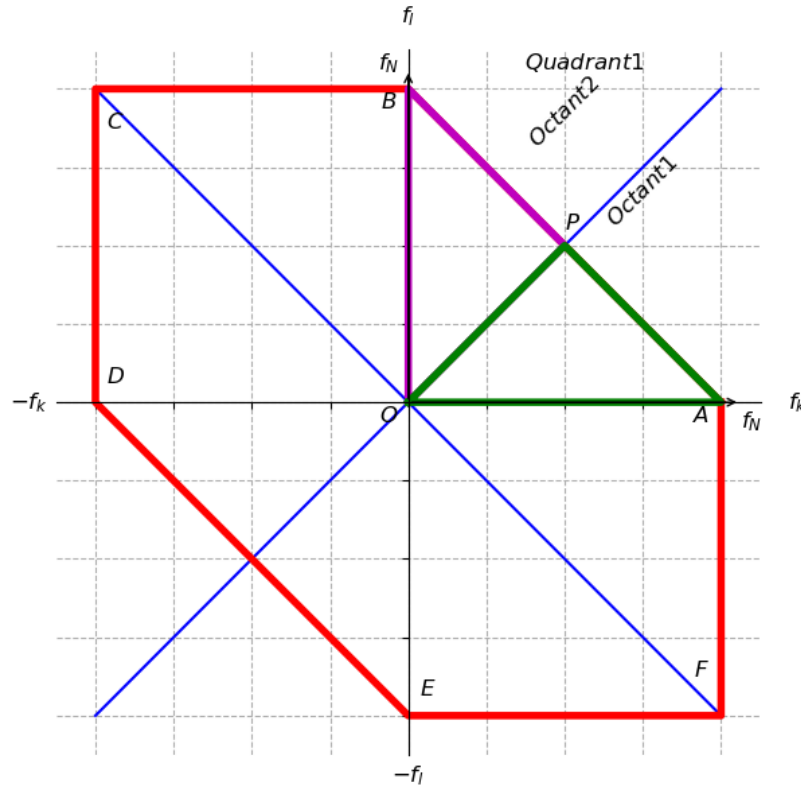


Figure A1: The hexagon $ABCDEF$ in the bicoherence plane. The regions $\triangle OPB$ (magenta) and $\triangle OPA$ (green) in Quadrant 1 are confined within the Nyquist frequency (f_N).

Appendix B. Similar Bicoherence Morphology

A few examples of glitches with similar morphology in the third-order statistic are shown in Fig. B1. The top row there displays the time-frequency maps of those glitches and is classified by Gravity Spy into the “extremely loud” and “koi fish” categories. The bottom row shows the corresponding bicoherence maps.

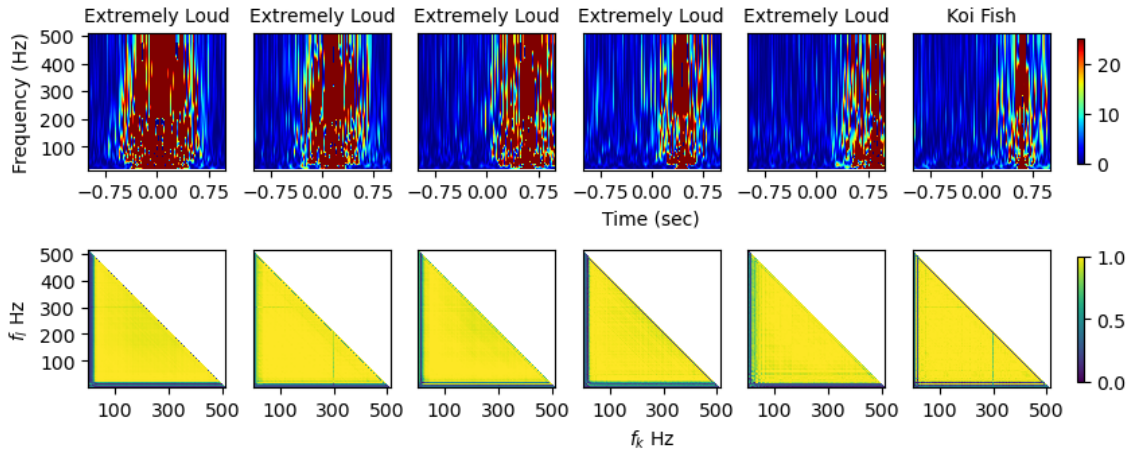


Figure B1: Top row: Spectrograms of “extremely loud” glitches (columns 1-5) and koi fish (column 6). Bottom row: Phase randomized bicoherence maps of corresponding glitches with 4sec data duration. Bicoherence maps in each sub-category of glitches reveal same phase-coupled bifrequencies, i.e., same bicoherence patterns, and suggest that the sources of these glitches are coupled in similar ways and manifested in the strain data.

Appendix C. Cross-bicoherence: A feasibility study

As noted above, the cross-bicoherence can help in finding the cause of glitches that arise due to the nonlinear coupling of disturbances of a pair of detector systems or components. However, cross-bicoherence is expensive to compute because it requires using pairs selected from hundreds of channels when little is known about the origins of a glitch. On the other hand, when some prior information is available on the origins, then the computational cost can be reasonable. For example, fast and slow scattered-light glitches and their origins are reasonably well understood [55, 56, 57]. Here, we pursue a feasibility study of cross-bicoherence with a small sample of slow scatter glitches.

One of the reasons for our choosing to study slow scatter glitches is that they are short-of a median duration ~ 3.2 -sec, which is of a timescale similar to the window we have tuned our bicoherence analysis on. The other reason is that their cause is now better understood: Low-frequency ground-motion, in the 0.03-0.1 Hz band, or microseismic noise, in the 0.1-0.3 Hz band (for slow scatter glitches) or anthropogenic noise in 1-6 Hz (fast scatter glitches) couple with high quality-factor resonances of the detector to create upconverted noise in the 10-100 Hz detector band that sometimes rises to frequencies as high as ~ 400 Hz [56]. Baffles that are installed in multiple places in the detectors to prevent scattered light from combining back with the main beam can actually play truant when not properly damped, and can amplify incident disturbances at their mechanical resonances. In particular, the cryo-manifold baffles

in Hanford and the arm cavity baffles in Livingston have been shown to be involved in causing the fast scatter glitches at those respective sites. On the other hand, light scattering from the annular end-reaction mass (AERM) and the transmission monitor system (TMS) have been implicated as the cause of slow scatter glitches.

In Fig. C1 we show the spectrograms (top panel) and bicoherence maps (bottom panel) of two of the slow scattering glitches in LIGO-Livingston during O3 that we studied. The spectrograms show the broadband power above ~ 16 Hz over a ~ 2 sec duration, as is characteristic of such glitches. However, they also show excess noise around 10 Hz, which is known to be due to scattered-light associated with noise coupling between end test mass (ETM) and TMS [55]. To compute the cross-bicoherences at those times, we take the $x(t)$ and $y(t)$ in Eq. (1) to be the L1:ASC-X_TR_A_NSUM_OUT_D channel, which is the most relevant scattered light witness channel that is also publicly available. We took $z(t)$ to be the strain channel. We compute the cross-bicoherence with the same input parameters as mentioned in Sec. 2. Interestingly, the neighborhood of that frequency in the bicoherence plots, i.e., $f_{k,l} \approx 10$ Hz, also shows significant bicoherence, which suggests the presence of nonlinear coupling. In a future work, we will report on a more elaborate investigation of noise couplings involved in scattered-light glitches, including the 10 Hz feature. The quest for improving low-frequency sensitivity to GW signals may benefit from the modeling and removal of such noise as well.

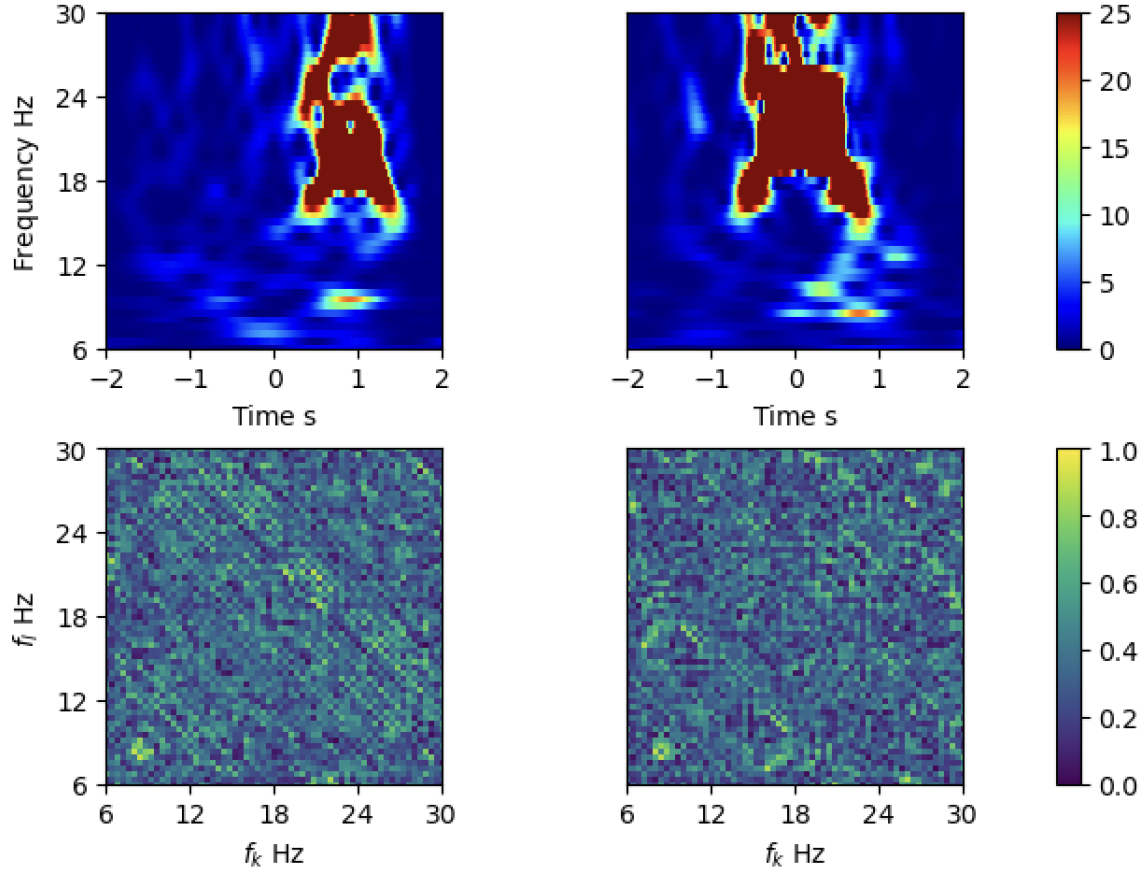


Figure C1: The spectrograms (top panel) and bicoherence maps (bottom panel) of two slow scattering glitches in LIGO-Livingston during O3. The spectrograms show the broadband power above ~ 16 Hz over a ~ 2 sec duration, as is characteristic of such glitches. The excess power at ~ 10 Hz is known to be due to scattered-light associated with ETM-TMS noise coupling [55]. The excess bicoherence at that frequency in the lower plots suggests the presence of nonlinear coupling and will be investigated in future.

References

- [1] G M Harry *et al* (LIGO Scientific Collaboration) 2010 *Classical and Quantum Gravity* **27** 084006 URL <http://stacks.iop.org/0264-9381/27/i=8/a=084006>
- [2] F Acernese *et al* 2014 *Classical and Quantum Gravity* **32** 024001 URL <https://doi.org/10.1088/0264-9381/32/2/024001>
- [3] T Akutsu *et al* (KAGRA Collaboration) 2020 Overview of kagra : Kagra science (*Preprint* 2008.02921)
- [4] B P Abbott *et al* (LIGO Scientific Collaboration and Virgo Collaboration) 2019 *Phys. Rev. X* **9**(3) 031040 URL <https://link.aps.org/doi/10.1103/PhysRevX.9.031040>
- [5] R Abbott *et al* (LIGO Scientific Collaboration and Virgo Collaboration) 2021 *Phys. Rev. X* **11**(2) 021053 URL <https://link.aps.org/doi/10.1103/PhysRevX.11.021053>
- [6] R Abbott *et al* (The LIGO Scientific Collaboration and the Virgo Collaboration) 2021 Gwtc-2.1: Deep extended catalog of compact binary coalescences observed by ligo and virgo during the first half of the third observing run (*Preprint* 2108.01045) URL <https://arxiv.org/abs/2108.01045>
- [7] R Abbott *et al* (The LIGO Scientific Collaboration and the Virgo Collaboration and the KAGRA Collaboration) 2021 Gwtc-3: Compact binary coalescences observed by ligo and virgo during the second part of the third observing run (*Preprint* 2111.03606) URL <https://arxiv.org/abs/2111.03606>
- [8] J Aasi *et al* (LIGO Scientific Collaboration and Virgo Collaboration) 2015 *Classical and Quantum Gravity* **32** 074001 URL <http://stacks.iop.org/0264-9381/32/i=7/a=074001>
- [9] D Davis *et al* 2021 *Classical and Quantum Gravity* **38** 135014 URL <https://doi.org/10.1088/1361-6382/abfd85>
- [10] F Acernese, *et al* 2023 *Classical and Quantum Gravity* **40** 185005 URL <https://dx.doi.org/10.1088/1361-6382/acdf36>
- [11] Joshi P, Dhurkunde R, Dhurandhar S and Bose S 2021 *Phys. Rev. D* **103**(4) 044035 URL <https://link.aps.org/doi/10.1103/PhysRevD.103.044035>
- [12] Choudhary S, More A, Suyamprakasam S and Bose S 2023 *Phys. Rev. D* **107**(2) 024030 URL <https://link.aps.org/doi/10.1103/PhysRevD.107.024030>
- [13] J Aasi *et al* (LIGO Scientific Collaboration and Virgo Collaboration) 2015 *Classical and Quantum Gravity* **32** 115012 URL <http://stacks.iop.org/0264-9381/32/i=11/a=115012>
- [14] Nuttall L K (LIGO Scientific Collaboration and Virgo Collaboration) 2018 *Phil.Trans.R.Soc.A* **376** URL <https://doi.org/10.1098/rsta.2017.0286>
- [15] Berger B K 2018 *Journal of Physics: Conference Series* **957** 012004 URL <https://doi.org/10.1088%2F1742-6596%2F957%2F1%2F012004>
- [16] Bose S, Dhurandhar S, Gupta A and Lundgren A 2016 *Phys. Rev. D* **94**(12) 122004 URL <https://link.aps.org/doi/10.1103/PhysRevD.94.122004>
- [17] Ajith P, Isogai T, Christensen N, Adhikari R X, Pearlman A B, Wein A, Weinstein A J and Yuan B 2014 *Phys. Rev. D* **89**(12) 122001 URL <https://link.aps.org/doi/10.1103/PhysRevD.89.122001>
- [18] Bose S, Hall B, Mazumder N, Dhurandhar S, Gupta A and Lundgren A 2016 *Journal of Physics: Conference Series* **716** 012007 URL <https://doi.org/10.1088%2F1742-6596%2F716%2F1%2F012007>
- [19] Costa C F D S, Billman C, Effler A, Klimenko S and Cheng H P 2018 *Classical and Quantum Gravity* **35** 055008 URL <https://doi.org/10.1088%2F1361-6382%2Faaa536>
- [20] Ormiston R, Nguyen T, Coughlin M, Adhikari R X and Katsavounidis E 2020 *Phys. Rev. Research* **2**(3) 033066 URL <https://link.aps.org/doi/10.1103/PhysRevResearch.2.033066>
- [21] Vajente G, Huang Y, Isi M, Driggers J C, Kissel J S, Szczepańczyk M J and Vitale S 2020 *Phys. Rev. D* **101**(4) 042003 URL <https://link.aps.org/doi/10.1103/PhysRevD.101.042003>
- [22] Hall B R 2019 *LIGO Detector characterization through higher order statistics and the development of the bicoherence tool for the LSC* Master's thesis Washington State University, Department of Physics and Astronomy Pullman, USA

- [23] Kim Y C and Powers E J 1979 *IEEE Transactions on Plasma Science* **7** 120–131
- [24] Fackrell J W A and McLaughlin S 1995 Quadratic phase coupling detection using higher order statistics *IEE Colloquium on Higher Order Statistics in Signal Processing: Are They of Any Use?* pp 9/1–9/8 ISSN null
- [25] Kim T 2008 *Polyspectral Signal Analysis Techniques for Interharmonics in Shipboard Power Systems* Ph.D. thesis The University of Texas Austin, USA
- [26] Hagihira S, Takashina M, Mori T, Mashimo T and Yoshiya I 2001 *Anesthesia and Analgesia* **93**(4) 966–970 URL <https://pubmed.ncbi.nlm.nih.gov/11574365/>
- [27] Elgar S and Sebert G 1989 *Journal of Geophysical Research: Oceans* **94** 10993–10998 URL <https://agupubs.onlinelibrary.wiley.com/doi/abs/10.1029/JC094iC08p10993>
- [28] B P Abbott *et al* 2016 *Classical and Quantum Gravity* **33** 134001 URL <https://doi.org/10.1088/0264-9381/33/13/134001>
- [29] M Zevin *et al* 2017 *Classical and Quantum Gravity* **34** 064003 URL <https://doi.org/10.1088/2F1361-6382%2Faa5cea>
- [30] Gwosc URL <https://www.gw-openscience.org/acknowledgement/>
- [31] Robinet F, Arnaud N, Leroy N, Lundgren A, Macleod D and McIver J 2020 *SoftwareX* **12** 100620 ISSN 2352-7110 URL <https://www.sciencedirect.com/science/article/pii/S2352711020303332>
- [32] J Glanzer *et al* 2023 *Classical and Quantum Gravity* **40** 065004 URL <https://dx.doi.org/10.1088/1361-6382/acb633>
- [33] Cabero M, Lundgren A, Nitz A H, Dent T, Barker D, Goetz E, Kissel J S, Nuttall L K, Schale P, Schofield R and Davis D 2019 *Classical and Quantum Gravity* **36** 155010 URL <https://doi.org/10.1088/2F1361-6382%2Fab2e14>
- [34] Davis D 2018 A 2019 aligo lho logbook URL <https://alog.ligo-wa.caltech.edu/aLOG/index.php?callRep=41263>
- [35] Ruxandra Bondarescu, Andrew Lundgren, Ronaldas Macas 2023 *ArXiv* URL <https://arxiv.org/abs/2309.06594>
- [36] B P Abbott *et al* (LIGO Scientific Collaboration and Virgo Collaboration) 2016 *Phys. Rev. Lett.* **116**(6) 061102 URL <https://link.aps.org/doi/10.1103/PhysRevLett.116.061102>
- [37] Nielsen A B, Nitz A H, Capano C D and Brown D A 2019 *Journal of Cosmology and Astroparticle Physics* **2019** 019–019 URL <https://doi.org/10.1088/1475-7516/2019/02/019>
- [38] LSC and VSC 2019 Power spectral densities (psd) release for gwtc-1 URL <https://dcc.ligo.org/LIGO-P1900011/public>
- [39] Bohé A *et al.* 2017 *Phys. Rev. D* **95** 044028 (Preprint 1611.03703)
- [40] Abbott B P *et al.* (LIGO Scientific, Virgo) 2019 *Phys. Rev. X* **9** 031040 (Preprint 1811.12907)
- [41] Mogushi K 2021 *Classical and Quantum Gravity* **38** 155004 URL <https://dx.doi.org/10.1088/1361-6382/ac08a7>
- [42] LSC and VSC O2 h1 noise lines URL https://www.gw-openscience.org/static/specclines/o2/O2LinesToBeCleaned_H1_v2.txt
- [43] LSC and VSC O3 h1 noise lines URL https://dcc.ligo.org/public/0176/T2100200/002/O3H1lines_gated_v1_7.csv
- [44] LSC and VSC O2 l1 noise lines URL https://www.gw-openscience.org/static/specclines/o2/O2LinesToBeCleaned_L1_v2.txt
- [45] LSC and VSC O3 l1 noise lines URL https://dcc.ligo.org/public/0176/T2100200/002/O3L1lines_gated_v1_7.csv
- [46] Van Rossum G and Drake F L 2009 *Python 3 Reference Manual* (Scotts Valley, CA: CreateSpace) ISBN 1441412697
- [47] Pybico: A python based bicoherence analysis package for gravitational wave data: Package is yet to be released
- [48] Duncan Macleod, *et al* 2019 *gwpv/gwpy: 0.14.2* URL <https://doi.org/10.5281/zenodo.2603187>
- [49] Alex Nitz *et al* 2020 *gwastro/pycbc: PyCBC release v1.16.11* URL <https://doi.org/10.5281/>

- [zenodo.4134752](https://zenodo.org/record/4134752)
- [50] Hunter J D 2007 *Computing In Science & Engineering* **9** 90–95
 - [51] Virtanen, *et al* and *SciPy 10 Contributors* 2020 *Nature Methods* **17** 261–272
 - [52] Charles R Harris, *et al* 2020 *Nature* **585** 357–362 URL <https://doi.org/10.1038/s41586-020-2649-2>
 - [53] Collaboration A 2013 *A&A* **558** A33 URL <https://doi.org/10.1051/0004-6361/201322068>
 - [54] Andrew Collette *et al* 2018 *h5py/h5py* 2.9.0 URL <https://doi.org/10.5281/zenodo.2439443>
 - [55] S Soni *et al* 2021 *Classical and Quantum Gravity* **38** 025016 URL <https://doi.org/10.1088/1361-6382/abc906>
 - [56] Siddharth Soni, Jane Glanzer, Anamaria Effler, Valera Frolov, Gabriela González, Arnaud Pele, Robert Schofield 2023 *ArXiv* URL <https://arxiv.org/abs/2311.05730>
 - [57] Tolley A E, Davies G S C, Harry I W and Lundgren A P 2023 *Classical and Quantum Gravity* **40** 165005 URL <https://dx.doi.org/10.1088/1361-6382/ace22f>